

# Magnetic Proximity-Induced Superconducting Diode Effect and Infinite Magnetoresistance in van der Waals Heterostructure

Jeacheol Shin<sup>1†</sup>, Suhan Son<sup>1,2†</sup>, Jonginn Yun<sup>1†</sup>, Giung Park, Kaixuan Zhang<sup>1,2</sup>, Young Jae Shin<sup>3,4</sup>, Je-Geun Park<sup>1,2\*</sup>, and Dohun Kim<sup>1\*</sup>

<sup>1</sup> *Department of Physics and Astronomy, and Institute of Applied Physics, Seoul National University, Seoul 08826, Korea*

<sup>2</sup> *Center for Quantum Materials, Seoul National University, Seoul, 08826, Korea*

<sup>3</sup> *Department of Physics, Harvard University, Cambridge, Massachusetts 02138, USA*

<sup>4</sup> *Center for Functional Nanomaterials, Brookhaven National Laboratory, Upton, New York 11973, USA*

<sup>†</sup>*These authors contributed equally to this work.*

<sup>\*</sup>*Corresponding author: jgpark10@snu.ac.kr, dohunkim@snu.ac.kr*

## Abstract

We report unidirectional charge transport in a  $\text{NbSe}_2$  noncentrosymmetric superconductor, which is exchange-coupled with a  $\text{CrPS}_4$  van der Waals layered antiferromagnetic insulator. The  $\text{NbSe}_2/\text{CrPS}_4$  bilayer device exhibits bias-dependent superconducting critical-current variations of up to 16%, with the magnetochiral anisotropy reaching  $\sim 10^5 \text{ T}^{-1}\text{A}^{-1}$ . Furthermore, the  $\text{CrPS}_4/\text{NbSe}_2/\text{CrPS}_4$  spin-valve structure exhibits the superconducting diode effect with critical-current variations of up to 40%. We also utilize the magnetic proximity effect to induce switching in the superconducting state of the spin-valve structure. It exhibits an infinite magnetoresistance ratio depending on the field sweep direction and magnetization configuration. Our result demonstrates a novel route for enhancing the nonreciprocal response in the weak external field regime (<50 mT) by exploiting the magnetic proximity effect.

Nonreciprocal charge transport, where the electrical resistivity varies depending on the current and magnetic-field direction, has attracted considerable attention over the past decade. Extensive experimental and theoretical research [1–12] has been conducted on systems with broken inversion or time-reversal symmetries. With notable recent progress, including the nonlinear Hall effect in Weyl semimetals [13,14] and chiral optical and electrical responses in semiconductors [2,15–17], efforts have been directed toward exploiting nonreciprocal transport in search of novel physical properties and functionalities.

In a system with both broken inversion and time-reversal symmetries, the nonlinear resistance  $R$  is in general measured to quantify the nonreciprocal transport, which is phenomenologically expressed as [1–3]

$$R = R_0(1 + \gamma IB), \quad (1),$$

where  $B$  represents the external magnetic field, and  $I$  denotes the electric current. The second term represents the nonreciprocal transport, which depends on the directions of both  $I$  and  $B$ . The coupling coefficient  $\gamma$ , which is known as magnetochiral anisotropy (MCA), defines the strength of the aforementioned dependence. Typical metals exhibit small MCA values ranging from  $10^{-3}$  to  $10^0$  T $^{-1}$  A $^{-1}$  because the spin–orbit interaction and magnetic energies are nominally far lower than the kinetic energy of the electrons, which is typically within a few electronvolts of the Fermi energy  $E_F$  [1,2,7,10]. However, measurement of the MCA in noncentrosymmetric superconducting materials such as transition-metal dichalcogenides (TMD) is a promising route for enhancing the MCA by orders of magnitude ( $\sim 10^4$  T $^{-1}$  A $^{-1}$  [4–6]) compared with the normal state, by replacing the role of  $E_F$  by superconducting gap [4,7]. Therefore, nonreciprocal charge transport is potentially suitable for developing phase-coherent and

direction-selective electronic devices, and a proof-of-principle demonstration has been performed for a broadband antenna [5].

The nonreciprocity quantified by the MCA generally arises from inequivalent resistances under different transport directions, which are usually finite. In contrast, exotic nonreciprocity can be achieved if the critical current becomes nonreciprocal. In such a case, the resistance is quenched for one direction while remaining finite for the other direction. If successful, this exotic nonreciprocity has considerable potential to be used for developing dissipation-less electric circuits [18]. The recent discovery of such a superconducting diode effect (SDE) in a Nb/V/Ta epitaxial film has prompted research on the nonreciprocal transport in superconductors [8]. In subsequent experiments, the SDE was observed in artificially nanofabricated systems such as a Josephson junction [19] and a noncentrosymmetric superconducting film with conformal-mapped nanoholes [20].

In general, nonreciprocal transport is observed using an external magnetic field for breaking time-reversal symmetry. Several studies have been performed on enhancing the MCA near the superconducting-normal state transition [21]. However, the commonly adopted approach typically requires a large magnetic field, on the order of a few teslas [4–6], which poses a challenge for practical application. This technical bottleneck provides a strong impetus to develop an alternative method for facilitating time-reversal symmetry breaking.

The proximity effect in superconductor and ferromagnet (S/F) heterostructures offers a possible solution to the requirement for a large magnetic field. In the case of a superconductor in close contact with a ferromagnet, the magnetic exchange field of the ferromagnet is expected to penetrate into the superconducting layer [22,23]. For example, the exchange field in the S-ferromagnet insulator (FI) heterostructure has been adequately understood based on this inverse proximity effect [24,25]. Exchange fields of a few teslas have often been observed in the spin splitting of the quasiparticle density of states in EuS/Al bilayers [26–28] and EuO/Al

bilayers [29]. This large exchange field paves the way for the development of novel superconducting spintronic devices. For instance, superconducting spin-valve structures exhibiting infinite magnetoresistance (MR) have been recently fabricated [30,31].

Here, we show that when a magnetic proximity-coupled van der Waals (vdW) heterostructure is used, the exchange field effectively reduces the otherwise large external magnetic field requirement while preserving or even enhancing the MCA in a noncentrosymmetric superconductor. Using a recently developed polymer-based strong adhesive transfer technique [32], we manufactured a  $\text{NbSe}_2/\text{CrPS}_4$  bilayer heterostructure and a  $\text{CrPS}_4/\text{NbSe}_2/\text{CrPS}_4$  trilayer spin-valve structure to leverage the magnetic proximity effect of the adjacent  $\text{CrPS}_4$  layer—an A-type layered antiferromagnetic insulator (AFI) below  $B \approx 0.7$  T [33,34]. The key observation was that a nonreciprocal SDE with a critical-current variation of up to 16% under a small external magnetic field of  $<50$  mT in the bilayer device and up to 40% in the trilayer device. Moreover, an infinite MR was obtained using the trilayer device under specific probe currents, which had never been demonstrated in a vdW heterostructure or S/A<sub>FI</sub> heterostructure.

As shown in Fig. 1a, the lattice structure of monolayer 2H- $\text{NbSe}_2$  possesses intrinsically broken in-plane inversion symmetry originating from inequivalent Nb and Se sites. Consequently, the itinerant electron of  $\text{NbSe}_2$  is subjected to an effective out-of-plane magnetic field through Ising-type spin-orbit coupling. This effective magnetic field causes the spin-dependent valley splitting of  $\text{NbSe}_2$  in Fig. 1b, as theoretically predicted [35] and experimentally confirmed using photoemission spectroscopy [36,37]. With locally broken inversion symmetry and spin-valley locking, the nonreciprocal behavior is expected to occur when the time-reversal symmetry is broken by a magnetic field perpendicular to the plane.

Fig. 1c shows an optical microscope image and a cross-sectional schematic of the  $\text{NbSe}_2/\text{CrPS}_4$  bilayer device fabricated using the polycaprolactone (PCL) dry-transfer

method [32]. Specifically, the 11 exfoliated layers of  $\text{NbSe}_2$  were picked up by the PCL stamp and dropped onto 6 layers of  $\text{CrPS}_4$  to minimize the polymer residue at the interface. Then, Ti (5 nm)/Au (70 nm) electrodes were evaporated after the conventional e-beam lithography. The  $\text{NbSe}_2$  with the odd number of layers was selected to exploit the broken spatial inversion symmetry to observe a nonreciprocal response. For example, we confirmed that a similar structure with an even number of  $\text{NbSe}_2$  layers does not show significant nonreciprocity (Supplementary Figure 1). The transport measurement was subsequently performed using a commercial variable temperature cryostat (Teslatron PT, Oxford Instruments) with a base temperature of  $T = 1.5 \text{ K}$ . We performed two different types of four-probe transport measurements in this study. The first was total resistance ( $R$  in Eqn. (1)) measurement using the direct-current voltage  $V$  with a Keithley 2182A Nanovoltmeter. The second measurement method involved using the first and second harmonic alternating-current (AC) resistances ( $R_0$  in Eq. (1) and nonlinear correction to  $R_0$  due to nonreciprocity, respectively) with a standard lock-in amplification technique (Signal Recovery, 7265). The device was field-cooled at  $B = 8 \text{ T}$  to increase the domain size of the  $\text{CrPS}_4$  layers [26,28,38–40].

Fig. 2a shows the  $I$ – $V$  characteristics of  $\text{NbSe}_2$  as a function of  $B$ . The distribution of the superconducting critical current  $I_c$  across the four quadrants of the colormap reveals broken symmetry in both the  $I$  and  $B$  directions. Fig. 2b shows the line cuts of the magnitudes of the  $I$ – $V$  curve in the vicinity of  $I_c$  under different  $B$  values, indicating the nonreciprocity of  $I_c$ . The observed  $I_c$  in the bilayer structure did not exhibit a significant change even when the current sweep direction is varied (inset of Fig. 2b). This suggests the effect from the retrapping current that an accidental Josephson junction could have caused can be disregarded. Fig. 2c shows the critical-current difference  $\Delta I_c$ , which is defined as the difference in  $I_c$  between the

positive ( $I_{c,+}$ ) and negative ( $I_{c,-}$ ) current-bias directions. The point symmetry of nonzero  $\Delta I_c$  exhibits clear magnetochirality. Furthermore,  $\%I_c$ , which is defined as

$$\%I_c = \frac{\Delta I_c}{\min(I_{c,+}, I_{c,-})} \times 100, \text{ reaches a value of up to } 16\% \text{ (inset of Fig. 2c).}$$

The second-harmonic resistance  $R_{2\omega}$  is shown as a function of  $B$  at different  $T$  values in Fig. 2d. The  $B$  field where the largest  $R_{2\omega}$  occurs generally coincides with that of  $\Delta I_c$ . The MCA can then be quantified using  $R_{2\omega}$ , as follows [4]:

$$\gamma = \frac{2R_{2\omega}}{R_0 BI}, \quad (2),$$

where the external field  $B$  is used to estimate  $\gamma$  solely from experimentally given conditions. Interestingly, Fig. 2e shows a  $\gamma$  value (MCA) of  $1.5 \times 10^5 \text{ T}^{-1}\text{A}^{-1}$  at  $T = 1.5 \text{ K}$ , mainly because of the reduced  $B$  field compared with that observed in previous studies [4–6]. A monotonic decrease in  $\gamma$  as a function of  $T$  is observed before  $\gamma$  becomes negligible at approximately 5 K, below the superconducting critical temperature  $T_c = 5.51 \text{ K}$  (inset of Fig. 2e) [41,42].

We ascribe this unusual behavior of  $R_{2\omega}$  to the magnetic ordering of CrPS<sub>4</sub>. As mentioned previously, A-type AFI CrPS<sub>4</sub> layers consist of antiferromagnetically coupled ferromagnetic monolayers for  $B < 0.7 \text{ T}$  at  $T = 1.5 \text{ K}$  [33,34]. Furthermore, because the proximity effect in the S/FI insulator is confined to the interface by the exponential decay of the electronic wave function in the insulator, the exchange coupling between the ferromagnetic CrPS<sub>4</sub> monolayer and NbSe<sub>2</sub> is expected to decay rapidly within the atomic distance [22,24,30]. Therefore, the antiferromagnetically coupled upper layers do not effectively offset the exchange field provided by the nearest ferromagnetic CrPS<sub>4</sub> monolayer, resulting in a significant exchange field dominated by the magnetization of the nearest monolayer. This

exchange field alone does not affect the orbital dynamics because the exchange field couples only with the quasiparticle spin and does not induce a Lorentz force.

Additionally, the antiferromagnetic nature of  $\text{CrPS}_4$  results in a negligible stray field [44]. Thus, the stray field of  $\text{CrPS}_4$  and the applied magnetic field do not provide the net magnetic field required to achieve the vortex flow regime, which is  $B > 2 \text{ T}$  for few-layer  $\text{NbSe}_2$  at a temperature of 2 K [5]. From this perspective, our observation of  $R_{2\omega}$  differs significantly from previously reported vortex dynamics-based  $R_{2\omega}$  on TMD. Indeed, in a recent study on  $R_{2\omega}$  in  $\text{NbSe}_2$  vdW devices, the  $R_{2\omega}$  peak appeared at  $B > 2 \text{ T}$  when  $T$  was 2 K, and the peak location tended to shift toward higher  $B$  values with the decreasing temperature [5]. But unlike these studies, we observed the  $R_{2\omega}$  peak at  $B \sim 10 \text{ mT}$ .

Having investigated the SDE observed in the  $\text{NbSe}_2/\text{CrPS}_4$  heterostructure, we next explore the response of the similar proximity-coupled structure with the increased exchange field by fabricating the  $\text{CrPS}_4/\text{NbSe}_2/\text{CrPS}_4$  trilayer spin valve structure shown in Fig. 3a. The device is fabricated using the previously mentioned PCL stamp technique, where the picked-up material stack was dropped directly onto pre-patterned  $\text{Pt}(18 \text{ nm})/\text{Ti}(2 \text{ nm})$  electrodes to avoid contamination.

Fig. 3b shows the current–voltage ( $I$ - $V$ ) characteristics of the device as a function of  $B$ , whose sweep direction is indicated in the upper-right corner. The colormap plots the magnetochirality, with nonreciprocity highlighted by the white dotted lines. Fig. 3c shows the critical-current difference  $\Delta I_c$ , which again shows a substantial value with the increased  $\%I_c$  value reaching 40% (inset of Fig. 3c). Furthermore, a significant change in  $I_c$  near  $B = 0 \text{ T}$  was observed, as shown in the enlarged plot of Fig. 3d. This change is also revealed in the averaged four-probe voltage measured by sweeping the magnetic field at  $I = 25 \mu\text{A}$  in Fig. 3e, with the noisy stochastic fluctuating behavior depicted in the background of the averaged

signal. This stochastic fluctuation may be related to the phase slip line (PSL) and kinematic vortices [45–47], the existence of the metastable state near the superconductor-normal state transition [48], or the domain structure of the proximity-coupled CrPS<sub>4</sub> and their dynamics to be discussed below. Nonetheless, the overall signal consistently showed the field-dependent switching behavior as shown in the averaged profile, demonstrating an infinite MR.

We note that the observed  $I_c$  change near  $B = 0$  T is related to the relative alignment of the adjacent CrPS<sub>4</sub> layer. As mentioned previously, CrPS<sub>4</sub> provides an effective exchange field with the dominant effect of the nearest ferromagnetic layer. Thus, the system can be effectively identified with a FI/S/FI trilayer structure, and the average exchange field on the quasiparticles is defined as follows:

$$\bar{h} = 2|\Gamma|S(a/d_s)\cos(\theta/2),$$

where  $|\Gamma|S$  represents the ferromagnetic spin multiplied by the coupling constant,  $\theta$  represents the angle between the magnetizations of the two ferromagnetic layers, and  $a$  and  $d_s$  represent the lattice constant and the thickness of the superconductor, respectively [24]. In our device, the coercive field of the nearest CrPS<sub>4</sub> layers is tuned according to their thicknesses. This condition allows the switching of the device between parallel (P) and antiparallel (AP) configurations through a gradual reduction in the magnetic field. Thus, in the P configuration ( $\theta = 0^\circ$ ), the net exchange field between two CrPS<sub>4</sub> layers results in a significant exchange field on NbSe<sub>2</sub>.

In contrast, in the AP configuration ( $\theta = 180^\circ$ ), the net exchange field on NbSe<sub>2</sub> is canceled out [30,31]. This magnetization reversal of the nearest CrPS<sub>4</sub> layers results in changing the exchange field on NbSe<sub>2</sub> near  $B = 0$  T considerably. Considering that the exchange field tends to reduce  $I_c$  because it disrupts the Cooper pairs, the analogous switching behavior of  $I_c$  near  $B = 0$  T reveals the exchange coupling between the NbSe<sub>2</sub>

and CrPS<sub>4</sub> layers, along with the hysteresis appearing in the colormap of Fig. 3d. This hysteresis becomes more apparent when the field is swept with the fixed current as in Fig. 3e, which could be distinguished from the stochastic fluctuation.

We now discuss the magnetic-field dependence of  $I_c$  in the colormap of Fig. 3b. The periodic modulation of  $I_c(B)$  can be due to either the Josephson effect or the change in the exchange field. A conventional explanation is that the Josephson effect causes the observed fluctuation of  $I_c$  as a Fraunhofer-like aperiodic oscillation. In such a case, the possible candidates for the Josephson weak link include the portion of the NbSe<sub>2</sub> in close contact with the CrPS<sub>4</sub>, resulting in an S-S'/F-S lateral Josephson junction [49,50]. The PSL is another candidate for the weak link [51]. However, the oscillation period requires the weak link responsible for the observed oscillation to be on the order of  $\sim 10^{-2} \mu\text{m}^2$ . Thus, for a  $\sim 4\text{-}\mu\text{m}$ -long device, the weak link must have a width of  $\sim 10 \text{ nm}$ . Our devices cannot satisfy these geometric conditions. Therefore, the oscillation is more likely to be caused by the oscillation of the exchange field, which is presumably caused by the magnetic domains and their dynamics. Further research is necessary to elucidate the domain-wall motion of CrPS<sub>4</sub>, particularly the domain structures of CrPS<sub>4</sub> and their dynamics.

In summary, we demonstrated that the magnetic proximity effect in the NbSe<sub>2</sub>/CrPS<sub>4</sub> heterostructure provides a large exchange field to induce clear nonreciprocal transport. The NbSe<sub>2</sub>/CrPS<sub>4</sub> bilayer device exhibited the SDE, where the magnetochiral  $\Delta I_c$  and  $R_{2\omega}$  were observed for  $B < 50 \text{ mT}$ , and  $\gamma$  reached  $\sim 10^5 \text{ T}^{-1}\text{A}^{-1}$ . We also observed an infinite MR and SDE in the CrPS<sub>4</sub>/NbSe<sub>2</sub>/CrPS<sub>4</sub> spin-valve structure, with  $\% I_c$  reaching  $\sim 40 \%$ . We expect the time-reversal symmetry breaking caused by the magnetic proximity effect to provide a novel route for investigating the potential application of nonreciprocal transport under small (or even zero) external magnetic fields.

## **Acknowledgments**

We thank Philip Kim and Gilho Lee for their valuable discussions. National Research Foundation of Korea supported this work (NRF) grants funded by the Korean Government (MSIT) (Nos. 2018R1A2A3075438, 2019M3E4A1080144, 2019M3E4A1080145, and 2019R1A5A1027055), the Creative-Pioneering Researchers Program through Seoul National University (SNU), and the Leading Researchers Program of the National Research Foundation of Korea (No. 2020R1A3B2079375).

## Figure captions

**Figure 1.** (a) Structure of non-centrosymmetric NbSe<sub>2</sub>. Inset: Side view of the structure of NbSe<sub>2</sub>, where the chirality is illustrated. (b) Schematic of the valley-dependent splitting (top) and the spin-valley locking of NbSe<sub>2</sub> (bottom). The broken inversion symmetry of NbSe<sub>2</sub> introduces spin-orbit coupling, which causes valley-dependent spin-orbit splitting ( $\Delta_{so}$ ). The Zeeman splitting ( $\Delta_z$ ) due to the downward magnetic field causes spin-valley locking. The Fermi surfaces of the spin branches are plotted with different colors. (c) Optical microscope image of the device. The boundaries of NbSe<sub>2</sub> and CrPS<sub>4</sub> flakes are marked with violet and green lines, respectively. Beneath the NbSe<sub>2</sub> were layers of antiferromagnetic CrPS<sub>4</sub>, which were placed on the top of the 285-nm-thick SiO<sub>2</sub> substrate. The Au electrodes were placed on the top of the NbSe<sub>2</sub>, and a four-probe measurement was conducted. The applied magnetic field was perpendicular to the substrate. The inset shows a schematic of the cross-section marked with the red dotted line.

**Figure 2.** (a) Voltage drop across the NbSe<sub>2</sub> layer with respect to the current and magnetic field at  $T = 1.55$  K. The nonreciprocity and magnetochirality appear as point symmetry, as indicated by the purple dotted line. (b)  $I$ - $V$  line cuts of Fig. 3a at 10, 20, 30, and 40 mT. The solid and dotted lines indicate the positive and negative transports direction, respectively. The line cuts are plotted near  $I_c$  to highlight the nonreciprocal  $I_c$ . The location of each curve in the colormap of Fig. 3a is marked with arrows of the same color. The inset shows the current-voltage characteristic with a different current sweep direction at  $B = 0$  T, where the arrows with the corresponding color indicate the current sweep direction. There is no noticeable

change in  $I_c$ , which suggests that the observed SDE is not by a retrapping current. **(c)** Dependence of  $\Delta I_c$  on the applied magnetic field. The measurement was performed by sweeping the magnetic field from positive to negative. The inset shows the dependence of  $\% I_c$  on the applied magnetic field. A maximum value of 16% was observed. **(d)** Magnetic-field dependence of the second-harmonic resistance. The magnetic field was swept from positive to negative. The temperature of each trace is indicated in the upper left legend. Magnetochirality was observed, and the peak location shifted to lower  $B$  values as the temperature increased. **(e)** MCA  $\gamma$  was calculated from Fig. 2d using Eq. (2) with the corresponding error bar. The inset shows the temperature dependence of the resistance of the device.

**Figure 3.** **(a)** Optical microscope image of the trilayer spin-valve device. The boundaries of  $\text{NbSe}_2$  and the top (bottom)  $\text{CrPS}_4$  flakes are marked with violet and green (purple) lines, respectively. Two antiferromagnetic  $\text{CrPS}_4$  layers sandwiched the  $\text{NbSe}_2$  layer, and the entire devices were placed on the top of the 285-nm-thick  $\text{SiO}_2$  substrate. The Au electrodes were at the bottom of the device, and a four-probe measurement was conducted. The applied magnetic field was perpendicular to the substrate. The inset shows a cross-sectional schematic illustrating the stacking sequence. **(b)** Colormap of the four-probe voltage with respect to the magnetic field and the current. The magnetic field was swept from positive to negative. A drastic change in  $I_c$  near  $B = 0 \text{ T}$  was observed. **(c)** Dependence of  $\Delta I_c$  on the applied magnetic field. The inset shows the dependence of  $\% I_c$  on the applied magnetic field. A maximum value of  $\sim 40\%$  was observed. **(d)** Magnified colormap of the four-probe voltage near  $B = 0 \text{ T}$ , where the magnetic field was swept from negative to positive (top) and from positive to negative (bottom). The significant change in  $I_c$  is clearly observed. This change produced a large MR under a

well-chosen probe current, such as  $I = 25 \mu\text{A}$  (black dotted line). Hysteresis was also observed, which reflects the effect of CrPS<sub>4</sub>. (e) Four-point voltage as a function of the magnetic field measured with a current magnitude of  $I = 25 \mu\text{A}$ , where the magnetic field was swept from positive to negative (red) and from negative to positive (black). The averaged signals of five traces are plotted, with each traces collectively plotted in the background with the lighter colors. The infinite MR and the hysteresis are clearly observed in the averaged curve. Stochastic switching also appears in each trace plotted in the background.

## References

- [1] G. Rikken and P. Wyder, *Magnetoelectric Anisotropy in Diffusive Transport*, Physical Review Letters **94**, 016601 (2005).
- [2] T. Ideue, K. Hamamoto, S. Koshikawa, M. Ezawa, S. Shimizu, Y. Kaneko, Y. Tokura, N. Nagaosa, and Y. Iwasa, *Bulk Rectification Effect in a Polar Semiconductor*, Nature Physics **13**, 578 (2017).
- [3] Y. Tokura and N. Nagaosa, *Nonreciprocal Responses from Noncentrosymmetric Quantum Materials*, Nature Communications **9**, 1 (2018).
- [4] R. Wakatsuki, Y. Saito, S. Hoshino, Y. M. Itahashi, T. Ideue, M. Ezawa, Y. Iwasa, and N. Nagaosa, *Nonreciprocal Charge Transport in Noncentrosymmetric Superconductors*, Science Advances **3**, e1602390 (2017).
- [5] E. Zhang, X. Xu, Y.-C. Zou, L. Ai, X. Dong, C. Huang, P. Leng, S. Liu, Y. Zhang, and Z. Jia, *Nonreciprocal Superconducting NbSe<sub>2</sub> Antenna*, Nature Communications **11**, 1 (2020).
- [6] Y. M. Itahashi, Y. Saito, T. Ideue, T. Nojima, and Y. Iwasa, *Quantum and Classical Ratchet Motions of Vortices in a Two-Dimensional Trigonal Superconductor*, Physical

Review Research **2**, 023127 (2020).

- [7] S. Hoshino, R. Wakatsuki, K. Hamamoto, and N. Nagaosa, *Nonreciprocal Charge Transport in Two-Dimensional Noncentrosymmetric Superconductors*, Physical Review B **98**, 054510 (2018).
- [8] F. Ando, Y. Miyasaka, T. Li, J. Ishizuka, T. Arakawa, Y. Shiota, T. Moriyama, Y. Yanase, and T. Ono, *Observation of Superconducting Diode Effect*, Nature **584**, 7821 (2020).
- [9] Y. M. Itahashi, T. Ideue, Y. Saito, S. Shimizu, T. Ouchi, T. Nojima, and Y. Iwasa, *Nonreciprocal Transport in Gate-Induced Polar Superconductor SrTiO<sub>3</sub>*, Science Advances **6**, eaay9120 (2020).
- [10] F. Pop, P. Auban-Senzier, E. Canadell, G. L. Rikken, and N. Avarvari, *Electrical Magnetochiral Anisotropy in a Bulk Chiral Molecular Conductor*, Nature Communications **5**, 1 (2014).
- [11] K. Yasuda, H. Yasuda, T. Liang, R. Yoshimi, A. Tsukazaki, K. S. Takahashi, N. Nagaosa, M. Kawasaki, and Y. Tokura, *Nonreciprocal Charge Transport at Topological Insulator/Superconductor Interface*, Nature Communications **10**, 1 (2019).
- [12] C. O. Avci, K. Garello, A. Ghosh, M. Gabureac, S. F. Alvarado, and P. Gambardella, *Unidirectional Spin Hall Magnetoresistance in Ferromagnet/Normal Metal Bilayers*, Nature Physics **11**, 570 (2015).
- [13] Q. Ma, S.-Y. Xu, H. Shen, D. MacNeill, V. Fatemi, T.-R. Chang, A. M. M. Valdivia, S. Wu, Z. Du, and C.-H. Hsu, *Observation of the Nonlinear Hall Effect under Time-Reversal-Symmetric Conditions*, Nature **565**, 337 (2019).
- [14] K. Kang, T. Li, E. Sohn, J. Shan, and K. F. Mak, *Nonlinear Anomalous Hall Effect in Few-Layer WTe 2*, Nature Materials **18**, 324 (2019).
- [15] J. E. Sipe and A. I. Shkrebtii, *Second-Order Optical Response in Semiconductors*, Physical Review B **61**, 5337 (2000).

- [16] N. Ogawa, M. Sotome, Y. Kaneko, M. Ogino, and Y. Tokura, *Shift Current in the Ferroelectric Semiconductor SbSI*, Physical Review B **96**, 241203 (2017).
- [17] K. F. Mak and J. Shan, *Photonics and Optoelectronics of 2D Semiconductor Transition Metal Dichalcogenides*, Nature Photonics **10**, 216 (2016).
- [18] T. Ideue and Y. Iwasa, *One-Way Supercurrent Achieved in an Electrically Polar Film*.
- [19] C. Baumgartner, L. Fuchs, A. Costa, S. Reinhardt, S. Gronin, G. C. Gardner, T. Lindemann, M. J. Manfra, P. E. F. Junior, and D. Kochan, *A Josephson Junction Supercurrent Diode*, ArXiv Preprint ArXiv:2103.06984 (2021).
- [20] Y.-Y. Lyu, J. Jiang, Y.-L. Wang, Z.-L. Xiao, S. Dong, Q.-H. Chen, M. V. Milošević, H. Wang, R. Divan, and J. E. Pearson, *Superconducting Diode Effect via Conformal-Mapped Nanoholes*, Nature Communications **12**, 1 (2021).
- [21] T. Ideue, S. Koshikawa, H. Namiki, T. Sasagawa, and Y. Iwasa, *Giant Nonreciprocal Magnetotransport in Bulk Trigonal Superconductor PbTa Se 2*, Physical Review Research **2**, 042046 (2020).
- [22] A. I. Buzdin, *Proximity Effects in Superconductor-Ferromagnet Heterostructures*, Reviews of Modern Physics **77**, 935 (2005).
- [23] S. Komori, A. Di Bernardo, A. I. Buzdin, M. G. Blamire, and J. W. Robinson, *Magnetic Exchange Fields and Domain Wall Superconductivity at an All-Oxide Superconductor-Ferromagnet Insulator Interface*, Physical Review Letters **121**, 077003 (2018).
- [24] P. G. De Gennes, *Coupling between Ferromagnets through a Superconducting Layer*, Physics Letters **23**, 10 (1966).
- [25] J. J. Hauser, *Coupling between Ferrimagnetic Insulators through a Superconducting Layer*, Physical Review Letters **23**, 374 (1969).
- [26] E. Strambini, V. N. Golovach, G. De Simoni, J. S. Moodera, F. S. Bergeret, and F. Giacotto, *Revealing the Magnetic Proximity Effect in EuS/Al Bilayers through*

- Superconducting Tunneling Spectroscopy*, Physical Review Materials **1**, 054402 (2017).
- [27] Y. M. Xiong, S. Stadler, P. W. Adams, and G. Catelani, *Spin-Resolved Tunneling Studies of the Exchange Field in EuS/Al Bilayers*, Physical Review Letters **106**, 247001 (2011).
- [28] X. Hao, J. S. Moodera, and R. Meservey, *Thin-Film Superconductor in an Exchange Field*, Physical Review Letters **67**, 1342 (1991).
- [29] P. M. Tedrow, J. E. Tkaczyk, and A. Kumar, *Spin-Polarized Electron Tunneling Study of an Artificially Layered Superconductor with Internal Magnetic Field: EuO-Al*, Physical Review Letters **56**, 1746 (1986).
- [30] B. Li, N. Roschewsky, B. A. Assaf, M. Eich, M. Epstein-Martin, D. Heiman, M. Münzenberg, and J. S. Moodera, *Superconducting Spin Switch with Infinite Magnetoresistance Induced by an Internal Exchange Field*, Physical Review Letters **110**, 097001 (2013).
- [31] Y. Zhu, A. Pal, M. G. Blamire, and Z. H. Barber, *Superconducting Exchange Coupling between Ferromagnets*, Nature Materials **16**, 195 (2017).
- [32] S. Son, Y. J. Shin, K. Zhang, J. Shin, S. Lee, H. Idzuchi, M. J. Coak, H. Kim, J. Kim, and J. H. Kim, *Strongly Adhesive Dry Transfer Technique for van Der Waals Heterostructure*, 2D Materials **7**, 041005 (2020).
- [33] Y. Peng, S. Ding, M. Cheng, Q. Hu, J. Yang, F. Wang, M. Xue, Z. Liu, Z. Lin, and M. Avdeev, *Magnetic Structure and Metamagnetic Transitions in the van Der Waals Antiferromagnet CrPS4*, Advanced Materials **32**, 2001200 (2020).
- [34] S. Ding, Y. Peng, M. Xue, Z. Liu, Z. Liang, W. Yang, Y. Sun, J. Zhao, C. Wang, and S. Liu, *Magnetic Phase Diagram of CrPS4 and Its Exchange Interaction in Contact with NiFe*, Journal of Physics: Condensed Matter **32**, 405804 (2020).
- [35] Z. Y. Zhu, Y. C. Cheng, and U. Schwingenschlögl, *Giant Spin-Orbit-Induced Spin*

*Splitting in Two-Dimensional Transition-Metal Dichalcogenide Semiconductors*, Physical Review B **84**, 153402 (2011).

- [36] Y. Nakata, K. Sugawara, S. Ichinokura, Y. Okada, T. Hitosugi, T. Koretsune, K. Ueno, S. Hasegawa, T. Takahashi, and T. Sato, *Anisotropic Band Splitting in Monolayer NbSe 2: Implications for Superconductivity and Charge Density Wave*, Npj 2D Materials and Applications **2**, 1 (2018).
- [37] L. Bawden, S. P. Cooil, F. Mazzola, J. M. Riley, L. J. Collins-McIntyre, V. Sunko, K. W. B. Hunvik, M. Leandersson, C. M. Polley, and T. Balasubramanian, *Spin–Valley Locking in the Normal State of a Transition-Metal Dichalcogenide Superconductor*, Nature Communications **7**, 11711 (2016).
- [38] O. Hellwig, T. L. Kirk, J. B. Kortright, A. Berger, and E. E. Fullerton, *A New Phase Diagram for Layered Antiferromagnetic Films*, Nature Materials **2**, 112 (2003).
- [39] O. Hellwig, A. Berger, and E. E. Fullerton, *Domain Walls in Antiferromagnetically Coupled Multilayer Films*, Physical Review Letters **91**, 197203 (2003).
- [40] X. Hao, J. S. Moodera, and R. Meservey, *Spin-Filter Effect of Ferromagnetic Europium Sulfide Tunnel Barriers*, Physical Review B **42**, 8235 (1990).
- [41] L. G. Aslamasov and A. I. Larkin, *The Influence of Fluctuation Pairing of Electrons on the Conductivity of Normal Metal*, Physics Letters A **26**, 238 (1968).
- [42] X. Xi, Z. Wang, W. Zhao, J.-H. Park, K. T. Law, H. Berger, L. Forró, J. Shan, and K. F. Mak, *Ising Pairing in Superconducting NbSe 2 Atomic Layers*, Nature Physics **12**, 139 (2016).
- [43] D. Xiao, G.-B. Liu, W. Feng, X. Xu, and W. Yao, *Coupled Spin and Valley Physics in Monolayers of MoS 2 and Other Group-VI Dichalcogenides*, Physical Review Letters **108**, 196802 (2012).
- [44] V. Baltz, A. Manchon, M. Tsoi, T. Moriyama, T. Ono, and Y. Tserkovnyak,

*Antiferromagnetic Spintronics*, Reviews of Modern Physics **90**, 015005 (2018).

- [45] N. Paradiso, A.-T. Nguyen, K. E. Kloss, and C. Strunk, *Phase Slip Lines in Superconducting Few-Layer NbSe<sub>2</sub> Crystals*, 2D Materials **6**, 025039 (2019).
- [46] A. Andronov, I. Gordion, V. Kurin, I. Nefedov, and I. Shereshevsky, *Kinematic Vortices and Phase Slip Lines in the Dynamics of the Resistive State of Narrow Superconductive Thin Film Channels*, Physica C: Superconductivity and Its Applications **213**, 193 (1993).
- [47] G. R. Berdiyorov, M. V. Milošević, and F. M. Peeters, *Kinematic Vortex-Antivortex Lines in Strongly Driven Superconducting Stripes*, Physical Review B **79**, 184506 (2009).
- [48] Y. Chen, Y.-H. Lin, S. D. Snyder, A. M. Goldman, and A. Kamenev, *Dissipative Superconducting State of Non-Equilibrium Nanowires*, Nature Physics **10**, 567 (2014).
- [49] O. Vavra, W. Pfaff, and C. Strunk, *Planar S-(S/F)-S Josephson Junctions Induced by the Inverse Proximity Effect*, Applied Physics Letters **95**, 062501 (2009).
- [50] L. K. Lin, S. Y. Huang, J. H. Huang, and S. F. Lee, *Nb Lateral Josephson Junctions Induced by a NiFe Cross Strip*, Applied Physics Letters **101**, 242601 (2012).
- [51] S. Tran, J. Sell, and J. R. Williams, *Dynamical Josephson Effects in Nb Se 2*, Physical Review Research **2**, 043204 (2020).

## Figures

Figure 1

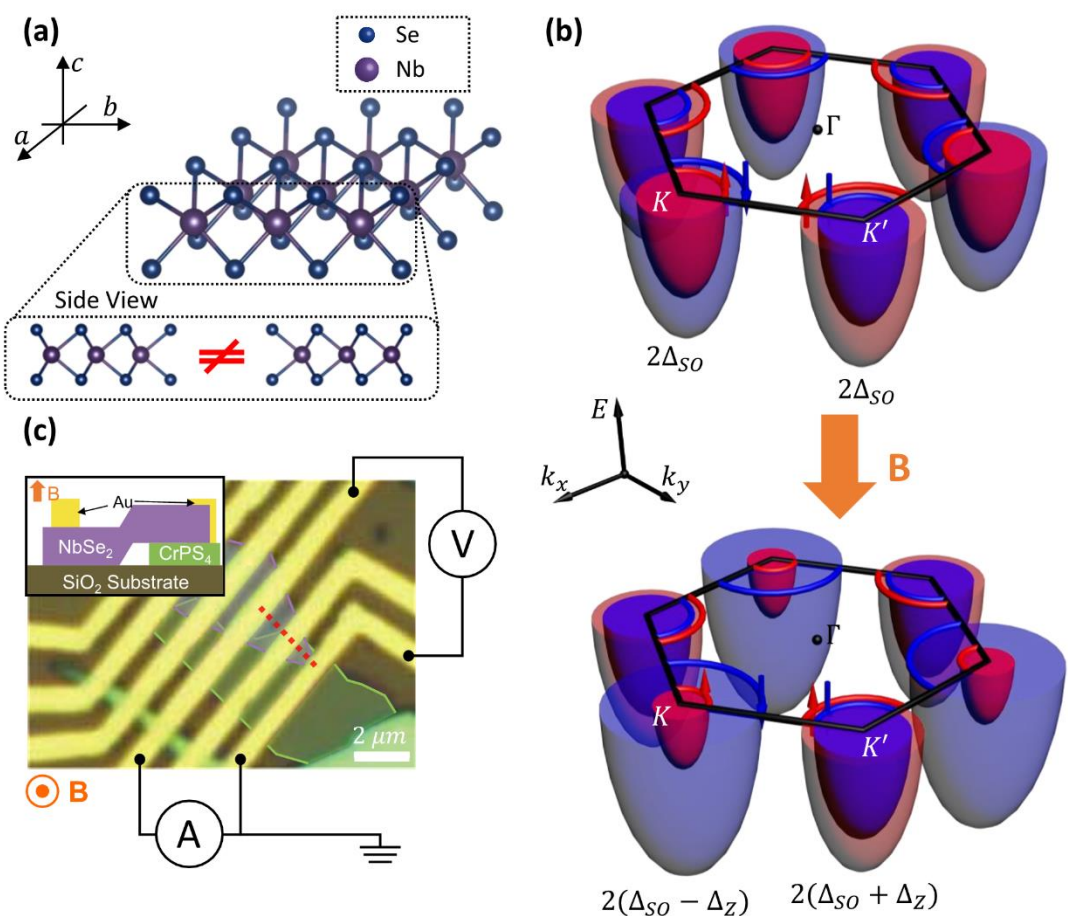


Figure 2

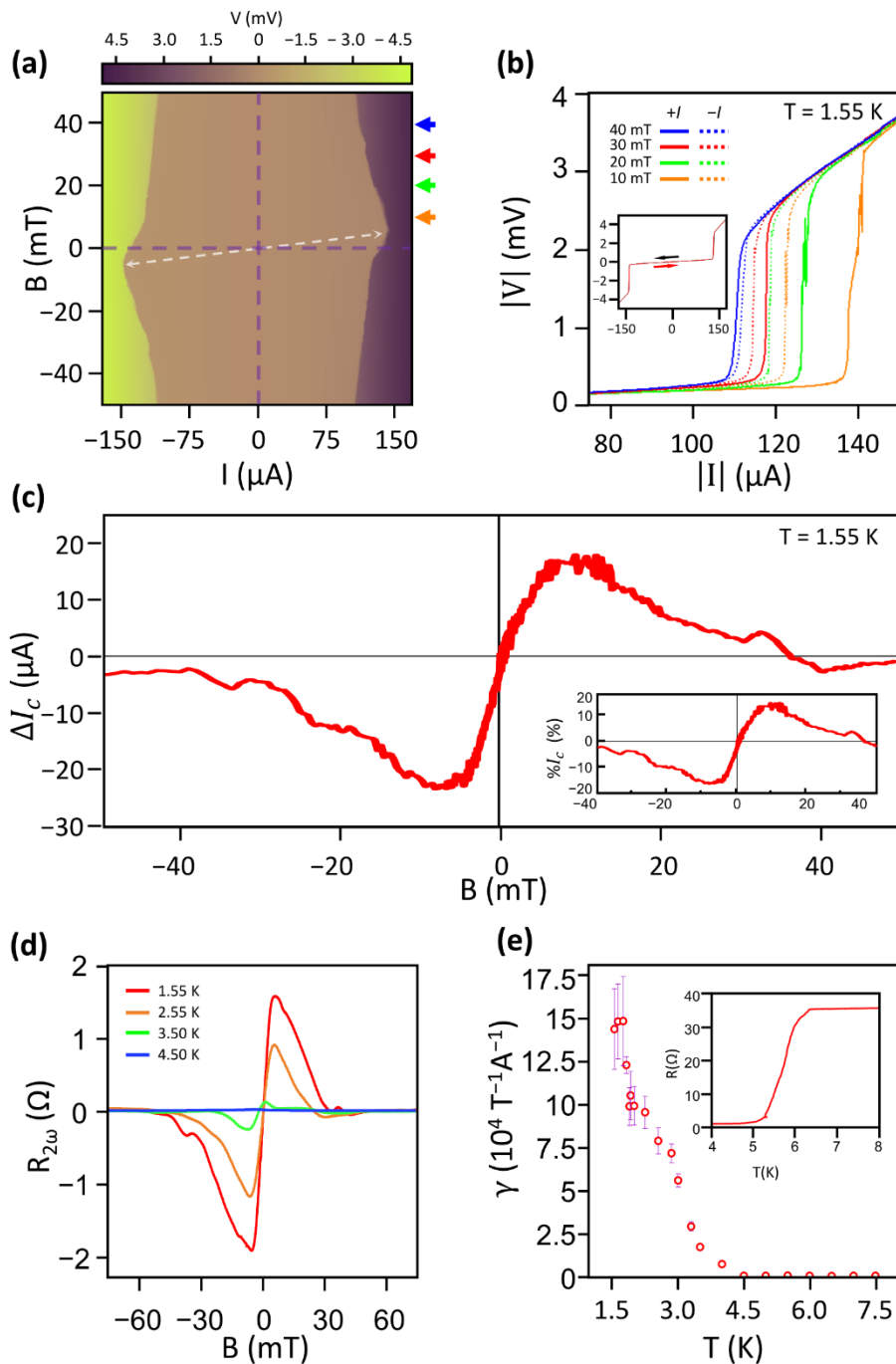
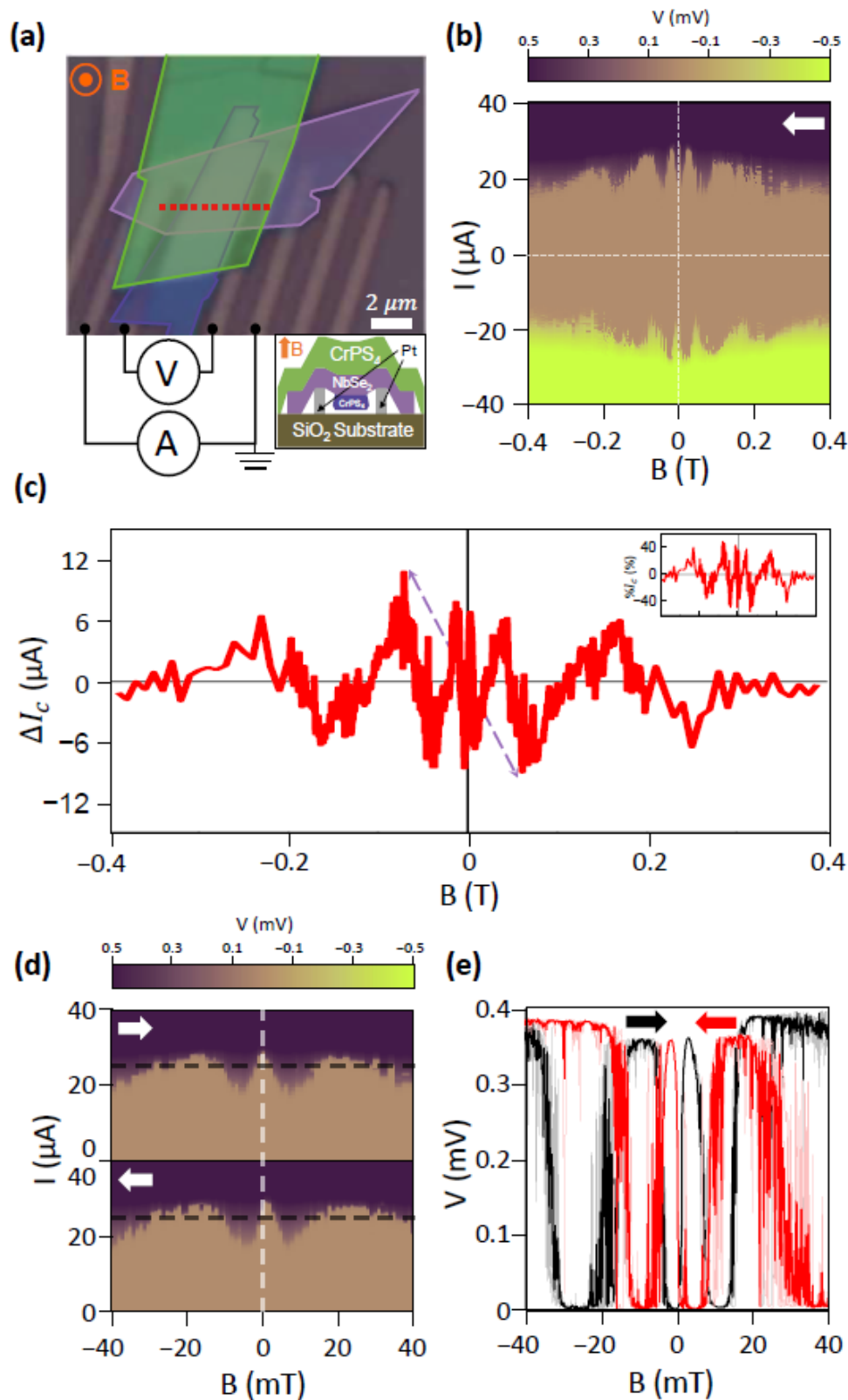


Figure 3



# Magnetic Proximity-Induced Superconducting Diode Effect and Infinite Magnetoresistance in van der Waals Heterostructure

Jeacheol Shin<sup>1†</sup>, Suhan Son<sup>1,2†</sup>, Jonginn Yun<sup>1†</sup>, Giung Park, Kaixuan Zhang<sup>1,2</sup>, Young Jae

Shin<sup>3,4</sup>, Je-Geun Park<sup>1,2\*</sup>, and Dohun Kim<sup>1\*</sup>

<sup>1</sup> Department of Physics and Astronomy, and Institute of Applied Physics, Seoul National University, Seoul

08826, Korea

<sup>2</sup> Center for Quantum Materials, Seoul National University, Seoul, 08826, Korea

<sup>3</sup> Department of Physics, Harvard University, Cambridge, Massachusetts 02138, USA

<sup>4</sup> Center for Functional Nanomaterials, Brookhaven National Laboratory, Upton, New York 11973, USA

<sup>†</sup>These authors contributed equally to this work.

\*Corresponding author: [jgpark10@snu.ac.kr](mailto:jgpark10@snu.ac.kr); [dohunkim@snu.ac.kr](mailto:dohunkim@snu.ac.kr)

## Supplementary Figures

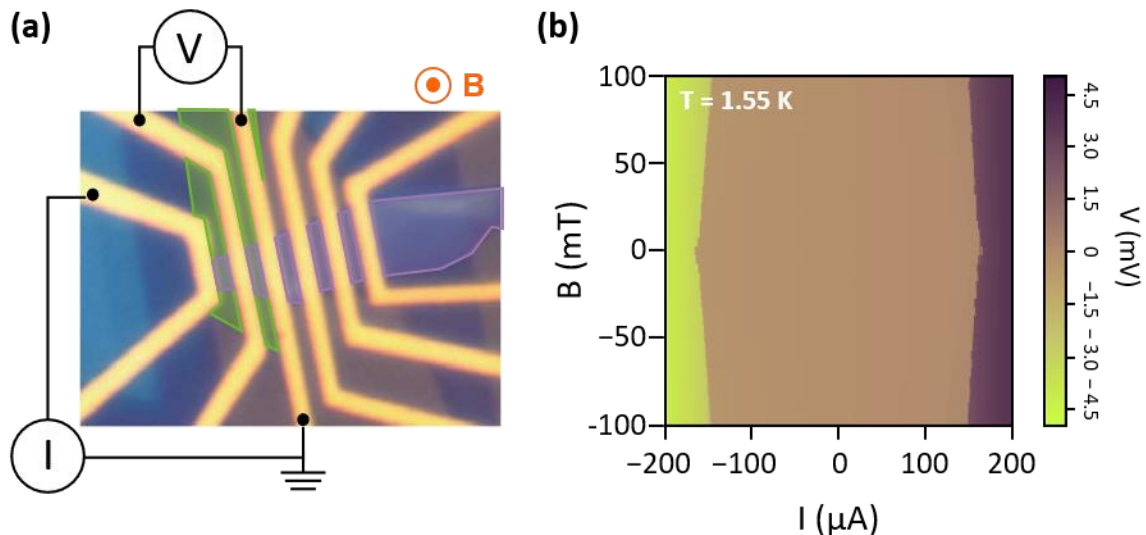


**Figure S1.** (a) Optical microscope image of 10 layers of the NbSe<sub>2</sub> device, where the inversion symmetry is globally preserved. The boundaries of NbSe<sub>2</sub> and CrPS<sub>4</sub> flakes are marked with purple and green lines, respectively. The Au electrodes were placed on the top of the NbSe<sub>2</sub>, and the four-probe measurement was conducted as illustrated in the schematic. The applied magnetic field was perpendicular to the substrate. (b) Colormap of the four-probe voltage with respect to the current and magnetic field at  $T = 1.55$  K. The result shows that the device with the even number of NbSe<sub>2</sub> layer does not show a significant nonreciprocity.

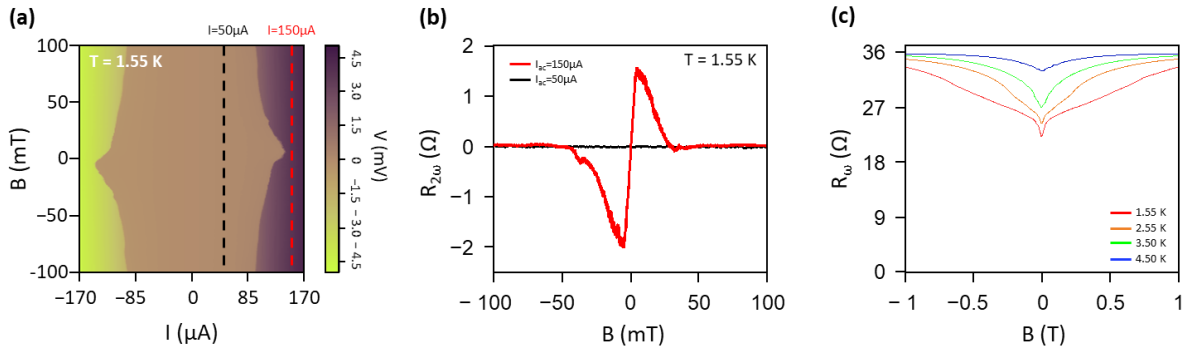


**Figure S2.** **(a)** Extended colormap of the four-probe voltage with respect to the current and magnetic field at  $T = 1.55$  K. The dotted lines indicate the amplitude of the AC bias to measure the second-harmonic resistance in Fig. S1b. **(b)** Measured second-harmonic resistance at two different current amplitudes:  $I_{ac} = 50 \mu$ A and  $I_{ac} = 150 \mu$ A. The magnetic field was swept from positive to negative. The signal disappeared when the amplitude decreased below  $I_c$ . **(c)** Measured first-harmonic resistance at a current amplitude of  $I_{ac} = 150 \mu$ A and different temperatures. The temperature of each curve is indicated in the bottom-right legend with the corresponding color. The first-harmonic resistance did not reach zero, even when the second-harmonic resistance did.

## Supplementary Discussion

We discuss that the observed behavior of  $R_{2\omega}(T)$  differs from that reported in previous research, where the primary source was either vortex dynamics below  $T_c$  [1–4] or the interplay of trigonal warping of the band structure and superconducting fluctuation near  $T_c$  [3,5,6]. These two mechanisms typically result in the nonreciprocity of the  $I$ – $V$  characteristics either near the vortex flow or in the superconducting fluctuation regime, producing an  $R_{2\omega}$  in AC measurements with a current amplitude smaller than the zero-field  $I_c$  [1,2,4,6]. Therefore,  $R_\omega$  should be completely quenched to zero whenever the  $R_{2\omega}$  signal disappears, unless the thermal creep of the vortex results in  $R_{2\omega}$  [1,2]. However, in our experiment, only the current amplitude exceeding the zero-field  $I_c$  yielded  $R_{2\omega}$  (Fig. 2d; Supplementary Figure 2), whose field dependence coincided with the behavior of  $\Delta I_c$ . Moreover,  $R_\omega$  did not completely decrease to zero even when  $R_{2\omega}$  did (Supplementary Figure 2), although the thermally activated vortex creep is possible only for  $T > 5.25$  K in NbSe<sub>2</sub> [1]. These behaviors indicate that the second-harmonic resistance shown in Fig. 2d reflects the nonreciprocity caused by the superconducting diode effect rather than the nonlinear resistance caused by vortex dynamics or superconducting fluctuation reported in the literature [1–4,6].

## Supplementary References

- [1] E. Zhang, X. Xu, Y.-C. Zou, L. Ai, X. Dong, C. Huang, P. Leng, S. Liu, Y. Zhang, and Z. Jia, *Nonreciprocal Superconducting  $NbSe_2$  Antenna*, *Nature Communications* **11**, 1 (2020).
- [2] Y. M. Itahashi, Y. Saito, T. Ideue, T. Nojima, and Y. Iwasa, *Quantum and Classical Ratchet Motions of Vortices in a Two-Dimensional Trigonal Superconductor*, *Physical Review Research* **2**, 023127 (2020).
- [3] R. Wakatsuki, Y. Saito, S. Hoshino, Y. M. Itahashi, T. Ideue, M. Ezawa, Y. Iwasa, and N. Nagaosa, *Nonreciprocal Charge Transport in Noncentrosymmetric Superconductors*, *Science Advances* **3**, e1602390 (2017).
- [4] T. Ideue, S. Koshikawa, H. Namiki, T. Sasagawa, and Y. Iwasa, *Giant Nonreciprocal Magnetotransport in Bulk Trigonal Superconductor  $PbTaSe_2$* , *Physical Review Research* **2**, 042046 (2020).
- [5] S. Hoshino, R. Wakatsuki, K. Hamamoto, and N. Nagaosa, *Nonreciprocal Charge Transport in Two-Dimensional Noncentrosymmetric Superconductors*, *Physical Review B* **98**, 054510 (2018).
- [6] D. Xiao, G.-B. Liu, W. Feng, X. Xu, and W. Yao, *Coupled Spin and Valley Physics in Monolayers of  $MoS_2$  and Other Group-VI Dichalcogenides*, *Physical Review Letters* **108**, 196802 (2012).